N87-16331

DUTY CYCLE TESTING AND PERFORMANCE EVALUATION OF THE SM-229 TELEOPERATOR*

Robert S. Stoughton** and Daniel P. Kuban+

This paper contains the first known experimental studies and analyses of teleoperator performance for specific duty cycles. The results are presented in two distinct areas as position usage patterns, and as three-dimensional power grids. The position usage patterns are a valuable means to assess the available motion range. The power grids are a unique concept for evaluating joint performance. Final conclusions contain recommendations to upgrade the teleoperator for optimum performance.

INTRODUCTION

This paper summarizes the results of work performed for the Consolidated Fuel Reprocessing Program at the Oak Ridge National Laboratory. An experimental analysis was conducted of the duties of a force-reflecting teleoperator system applied to a series of tasks. These tasks are typical for operations in a remote hazardous environment. The teleoperator system studied is one used in many applications in this country, the TeleOperator Systems (TOS) Model SM-229. In this experiment, the joint positions and motor currents were recorded at a rate of 10 Hz over 50 h of operation. This work provides general information about teleoperators that was previously unavailable, and that is useful in determining design parameters for improved systems. They provide insight into proper motor sizing, gear ratios, and drive configurations. The resulting analysis technique is generalized and shown to be a valuable tool for design analysis of operating and future systems.

*Research sponsored by the Office of Spent Fuel Management and Reprocessing Systems, U.S. Department of Energy, under contract No. DE-AC05-840R21400 with Martin Marietta Energy Systems, Inc.

**University of California, Santa Barbara.

+Oak Ridge National Laboratory Engineering Division, Oak Ridge, Tennessee.

EXPERIMENTAL SYSTEM

The experimental work described here was carried out in the Remote Systems Development Facility (RSDF) located at Oak Ridge National Laboratory (ORNL). This facility provided a realistic working environment for evaluating remote maintenance equipment. The design and makeup of this facility have been described previously.[1] A remote test area with the teleoperator slave arms, an operator control station, and a PDP 11/34 data acquisition system are the major components of the RSDF. The remote test area (Fig. 1) contains equipment for a variety of manipulation tasks considered to be the generic subtasks of more complex remote operations. The slave manipulator arms are mounted on the end of a telescoping hoist of a three-axis transporter, allowing the arms to travel anywhere within the remote cell. The operator control station (Fig. 2) contains the master arms, television screens for viewing the remote test area, and controls for the cameras, transporter, and auxiliary functions.

The teleoperator used was a TeleOperator Systems (TOS) Model SM-229, a force-reflecting system with a lift capacity of 10 kg per arm. The master arms and slave arms (Fig. 3) are kinematically identical. Figure 3 also shows the reference configuration of the manipulator, with the upper arm and end effector horizontal and forward, and the forearm vertical.

The shoulder pitch and roll motions are driven by two motors through a geared differential. This differential drive configuration allows the two motors to share equally the load in a pure pitch (or pure roll) motion. However, simultaneous pitch and roll loading results in unequal duty cycles in the two motors. The elbow pitch is gear driven by a single motor. The wrist yaw (or elbow roll) is driven by a single motor via metal tapes. The wrist pitch and roll are driven by two motors through a differential with the torque transferred via metal tapes passing over idlers in the elbow. The wrist yaw, wrist pitch/roll, and tong motors are mounted on the shoulder roll and the motors provide the mechanical counterbalance for the forearm. Gears in the elbow pitch drive rotate this motor package to balance the forearm.

Position data for the joints were measured by potentiometers within the arms, and motor current data were measured by precision shunt resistors within the control boxes. These signals were recorded with a PDP 11/34 at 10 Hz while operators performed selected manipulation tasks. Data were sampled for the right slave arm only, so all results presented pertain to the right slave arm. It was determined[2] that the right arm is used significantly more than the left, so this limitation was not considered detrimental.

EXPERIMENTAL TASKS

Five manipulation tasks were previously selected as being generic representations of remote maintenance operations:[1]

1. Removal/installation of an in-line instrument package. Using an impact wrench, loosen the clamp retaining the instrument package and disengage the pin connector from the instrument package.

2. Removal/installation of a 1/4-hp motor. Remove the motor with a lifting bale (see Fig. 4), assisted by an overhead hoist.

3. Removal/installation of a 76-cm pipe flange. Remove flange mounting bolts with the impact wrench and use the hoist to lift the flange (see Fig. 4).

4. Removal of a tubing service jumper with three horizontal connectors. Loosen the clamps with the impact wrench and remove the jumper.

5. Removal of a 15-cm pipe flange with two horizontal captured bolts. Loosen the captured bolts with the impact wrench and remove the flange.

Because the geometry and activity of tasks four and five are similar, this study considers their averaged data as one task. Tool-changing time is included in the task analysis, particularly the motion and time required to access the impact wrench.

Four experienced manipulator operators performed each task at least ten times. Data recording started when the operator began the task and ended immediately upon completion of the task or upon any equipment malfunction. A total of about 50 h of operational data were recorded in this manner.

The results presented here can be applied with certainty only to the specific tasks studied. Teleoperators perform a wide range of complex, unstructured tasks which cannot all be represented by the tasks that were studied here. The mobility of the transporter system does reduce some of the task-dependent effects because the operator can use any desired approach to the work site, and can use transporter movements to eliminate long reaches.

It was apparent that the wrist-pitch degree-of-freedom (DOF) was severely torque limited because just holding the impact wrench required nearly all of the available torque. This constraint made reassembly of the 15-cm pipe flange impossible because there was not enough torque remaining to manipulate the flange.

Full stall torque from the motors was not always available because of equipment limitations and drift in the analog control system (the brakes would energize when the position error of any joint exceeded a safety limit). The averaged torque that was available without exceeding this limit was measured daily. The available torque averaged for all seven motors was only about 75% of the full stall torque.

EXPERIMENTAL DATA AND DISCUSSION

The recorded data were compiled into arrays of joint positions and motor currents for each DOF, relative to the amount of time spent at that position and at that current. The position data were also transformed from joint position to wrist position and orientation in cartesian coordinates. The velocity data were derived from the position measurements relative to time, and the motor-current measurements were converted to motor torque. The three-dimensional mechanical power grid was developed to describe how the joint was exercised during the experiment. This plot shows torque and velocity combinations versus their total duration time normalized to the longest duration combination.

As each task had more than one trial, the arrays were accumulated to obtain a composite average of the trials. These data were then converted to percentages of total time. The data arrays for all five tasks were then averaged with equal weighting to obtain the final results. A complete discussion of the test procedures and equipment, and the results can be found in Ref. 3.

The first area that will be discussed is that of joint position usage. Figures 5 through 7 are histograms showing how the operators used the available motion range for some of the joints. The angular range of each plot corresponds to the motion range of that joint, and the radius of each "pie slice" is proportional to the percentage of total time that the operator stayed in that part of the motion range. To visualize the wrist roll histogram (Fig. 7), one must consider the tong to be holding a pin or bar such that it is vertical in the reference configuration. The plot represents the orientation of that pin with respect to the wrist.

These figures (5 through 7) also provide very useful data for analyzing usage. Of more general interest is the working volume of human-controlled manipulation as applied to the generic tasks. These data are given in Figs. 8 through 10 as histograms of the position of the wrist pivot in cartesian coordinates. Figure 11 combines the histogram data of the wrist pitch and yaw as wrist orientation. In each plot, the darkest blocks are the most frequently used areas. Progressively lighter areas are less frequently used (geometric progression of 0.6), and the lightest shades represent blocks in which the wrist position was less than 1% of the time spent in the most used block.

Table 1. Mean Positions in Joint Coordinates

JOINT	MEAN OPERATING POSITION	REFERENCE POSITION (Figure 3)
Shoulder pitch	-9.8° (down)	0°
Shoulder roll	-13.0° (left)	0°
Elbow pitch	5.1° (forward)	0°
Elbow roll	42.5° (left)	0°
Wrist pitch	-17.7° (down)	0°
Wrist roll	4.0° (CCW from behind)	0°

Table 2. Mean Position in Cartesian Coordinates Measured From Shoulder Pivot

DIRECTION	MEAN WRIST POSITION (cm)	REFERENCE WRIST POSITION (Figure 3) (cm)
Vertical	10.77 (down)	10.63
Forward	8.74 (forward)	10.04
Transverse	1.88 (left)	0.0

The second area of discussion is that of how each joint was exercised. The three-dimensional mechanical power grids (Fig. 12, typical) were developed as an aid for analyzing the gear reductions and motor sizings. These grids were developed from the measured data and are valid only for this teleoperator configuration, and these specific tasks. The independent variables on these grids are the components of mechanical power: velocity and torque, scaled to the no-load speed and stall torque, respectively. Each variable is divided into 25 increments (4% of range) to form a 25 by 25 grid. The dependent variable is the log of the total operation time, scaled to the most used grid block. Thus, the height of each crosshair of the grid represents the log of the total operation time spent simultaneously within the velocity and torque ranges corresponding to that crosshair. Note that when the velocity and acceleration are in the same direction, the diagonal connecting stall torque and peak velocity is a physical limitation of the motor. Time can be spent above this diagonal only when the velocity and acceleration are in opposite directions.

This representative data collected from a working teleoperator system allows immediate understanding of the design margin and limitations within each joint. Figure 12 presents an idealized mechanical power grid for teleoperator joints. The most time is spent at 0 to 4% velocity and torque because the teleoperator is not moving and has no load, while the operator moves the transporter or adjusts the cameras. The grid represents desirable features by its symmetry about its main diagonal (good balance of speed and torque) and by reaching zero usage time just below 100% of torque and velocity capability (avoiding saturation). In an ideal power grid, the motor and gear reduction are adequate to meet all demands, but they are not significantly oversized.

The degree of symmetry in the grid provides a quantitative evaluation of the gear reduction. Figure 13 illustrates actual data from the wrist pitch DOF with the grid shape indicating a gear reduction that is too small. This gear reduction gives the joint a no-load speed in excess of that required and yet reduces the available stall torque to a level that hinders performance. In this DOF, high (% of max) velocities do not occur, while high torques occur regularly, as shown by the grid being skewed toward the torque axis. The opposite occurs when the gear reduction is too large. The joint could support torques greater than required but would be limited in velocity, shown by the grid being skewed toward the velocity axis.

The volume beneath the normalized grid and the points where the grid reaches zero along each axis provide data to evaluate motor sizing. Figures 14 and 15 show the grid shapes corresponding to a proper gear reduction, but with an oversized and undersized motor, respectively. These grids represent actual data from the shoulder roll and elbow pitch, respectively. When the motor is too large, the capacity in both torque and velocity is considerably greater than required, and the grid reaches zero at well below full capacity

with a small enclosed volume. Conversely, an undersized motor often operates at peak capacity in velocity or torque (the zero crossing is extrapolated beyond 100%) and the normalized grid encloses a large volume.

The power grid scales for the shoulder and wrist are special since they are driven by differentials. The torque/velocity capacity for one DOF in a differential drive varies with the simultaneous torque/velocity of the other DOF. The torque/velocity grids are scaled to the maximum possible values (i.e., when both motors drive the same DOF). The scaling causes the shoulder power grids to appear to be the result of oversized motors. The shoulder roll power grid (Fig. 14) is relatively symmetrical but reaches zero at well below full capacity. If simultaneous pitch and roll torques/velocities could be avoided, smaller motors could be used. The elbow pitch power grid (Fig. 15) encloses a relatively large volume with significant times spent at near 100% of torque and at near 100% of velocity. A motor 10 to 15% larger is required to allow both needs to be met. The wrist pitch and roll power grids (Figs. 13 and 16) are each skewed toward the torque axis and high velocities are never used. The time at high torque is particularly significant because of the differential drives. The high torque indicates that large gear reductions are needed, but this is limited by the load capacity of the metal tapes.

In the past, teleoperator joint gear reductions have been determined using the concept of effective radius, which is the direct-drive lever arm at which the stalled motor torque will support the design capacity. For example, a motor with a stall torque of 4 N·m used to support an 80-N capacity has an effective radius, ρ, of 0.05 m. The gear reductions for the joints are determined by dividing the maximum joint length, L, by the effective radius and the number of motors, N, that are driving that joint (i.e., two for differentials):

$$R = L/\rho N$$

Past designs have consistently used this formula for all joints but the results of this report indicate that some design revisions are now appropriate. Table 3 presents the joint lengths and gear reductions based on an effective radius and the suggested improved gear reductions based on the experimental evaluation. This would be of tremendous value if this evaluation was made on a prototype unit and then implemented on the production units.

The improved gear reductions are based on matching the zero crossings on the torque and velocity axes. In some cases, the measured zero crossings had to be extrapolated beyond 100%. For the wrist pitch, a somewhat larger increase than the stated 40% may be needed, as the wrist pitch was incapable of supporting the torque needed to reassemble the 15-cm flange.

Table 3. Joint Lengths and Gear Reductions

JOINT	LENGTH AT FULL EXTENSION (cm)	ACTUAL GEAR REDUCTION BASED ON ρ [a]	IMPROVED GEAR REDUCTION BASED ON EXPERIMENTAL DATA
Shoulder pitch[b]	142	40	43.3
Shoulder roll[b]	58	29.4	30.6
Elbow pitch	84	43.5	39.6
Wrist yaw	15	8	8.9
Wrist pitch[b]	15	3.9[c]	7.7
Wrist roll[b]	12	3.3	5.1

[a]90-N capacity, T_{stall} = 1.71 N•m (continuous) ρ = 1.9 cm.

[b]Differential drive.

[c]Select worst case for differential; second gear reduction is then adjusted for actual gear selection by choice of differential output gear.

CONCLUSIONS

The duty cycles of a human-controlled manipulator have been experimentally measured. The time-use histograms of the kinematic range reveal specific improvements can be made in the joint motion ranges of the TOS Model SM-229. The working volume of the teleoperator can be applied to the design of all human-controlled manipulators. The mounting configuration of teleoperators must be designed to optimally fit the volumetric coverage to the working volume, and the drive configurations must operate most effeciently within the working volume for the anticipated tasks.

A graphical method for optimizing joint velocity and torque capabilities has been developed. This method, based on three-dimensional time-use histograms of mechanical power usage, was applied to the measured duty cycle data to determine optimal motor sizing and gear ratio selection for this human-controlled system.

REFERENCES

1. M. Clarke, W. Hamel, and J. Draper, "Human Factors in Remote Control Engineering," pp 8-16 in Proceedings 31st Conference on Remote Systems Technology, American Nuclear Society, 1983.
Nuclear Society, 1983.

2. J. V. Draper and M. M. Clarke, personal communication, October 1983.

3. R. S. Stoughton, "Kinematics and Duty Cycles of the SM-229 Force Reflecting Servomanipulator," M.S. thesis, The University of Tennessee, Knoxville, 1985.

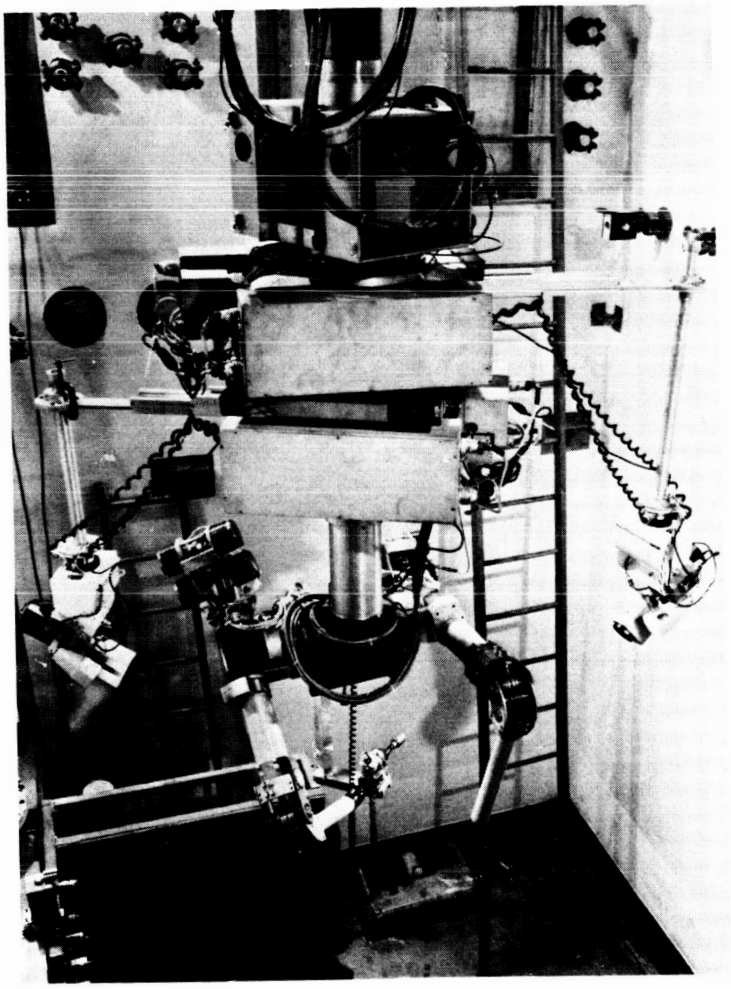

Figure 1. - Slave manipulator arms and remote cell.

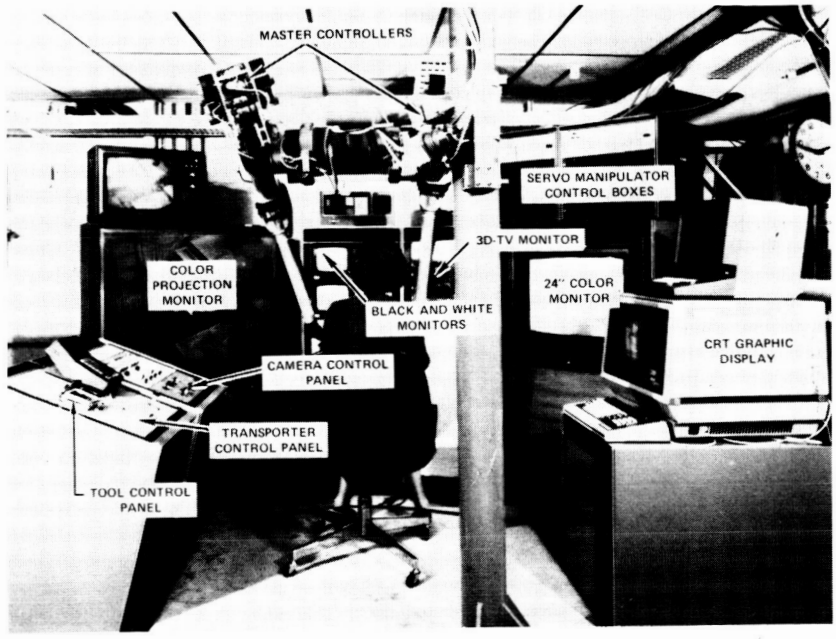

Figure 2. - Operator control station.

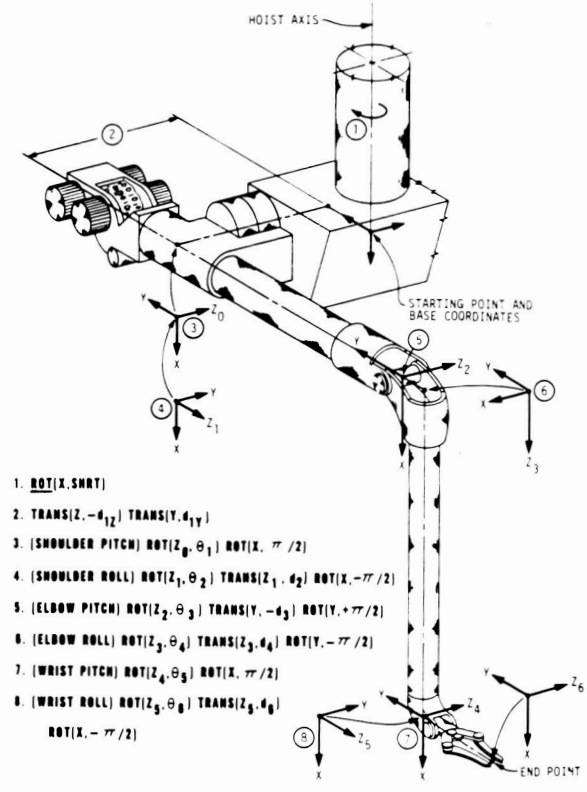

Figure 3. - Manipulator kinematics.

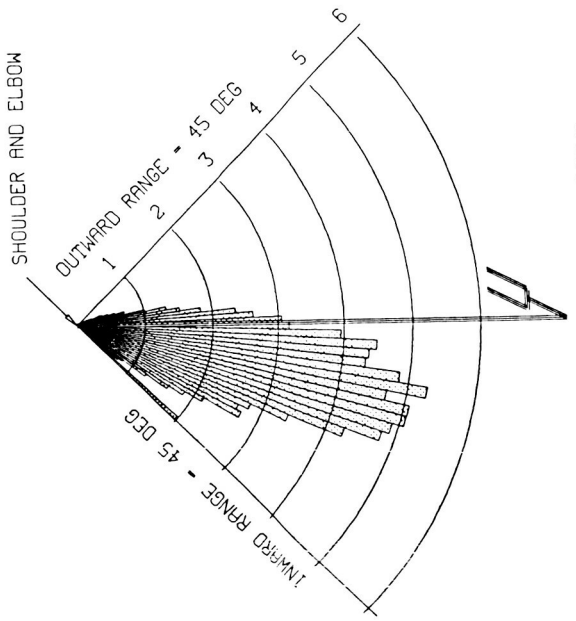

Figure 5. - Range of shoulder roll position usage.

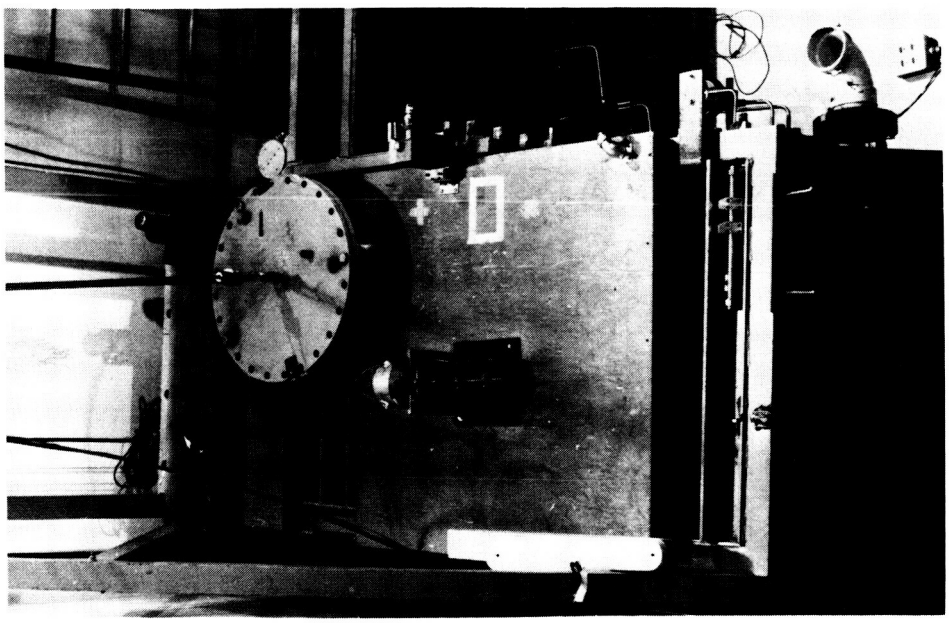

Figure 4. - Motor mount and 76-cm pipe flange.

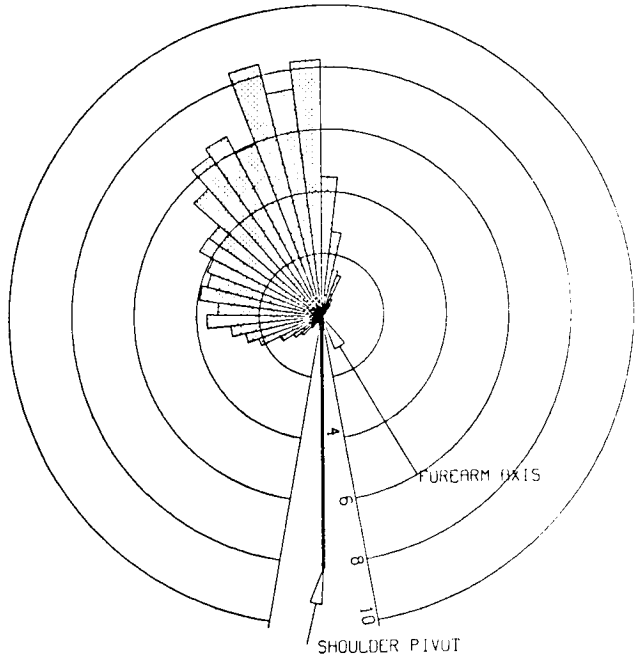

Figure 6. - Range of elbow roll (Yaw) position usage.

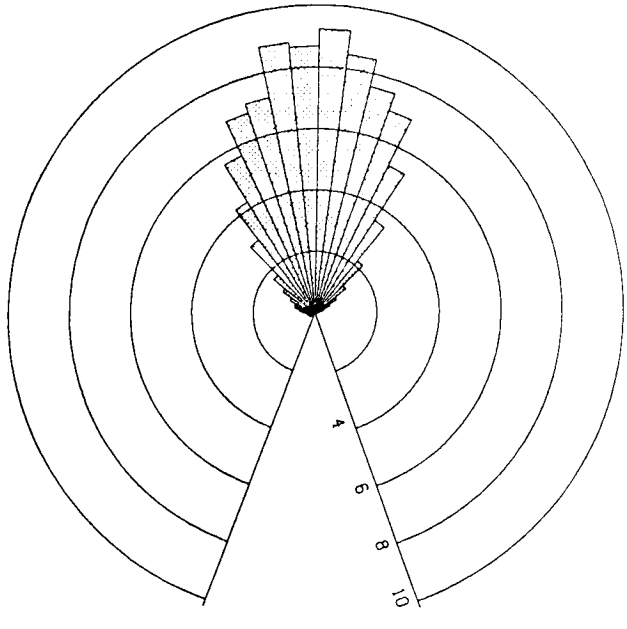

Figure 7. - Range of wrist roll position usage.

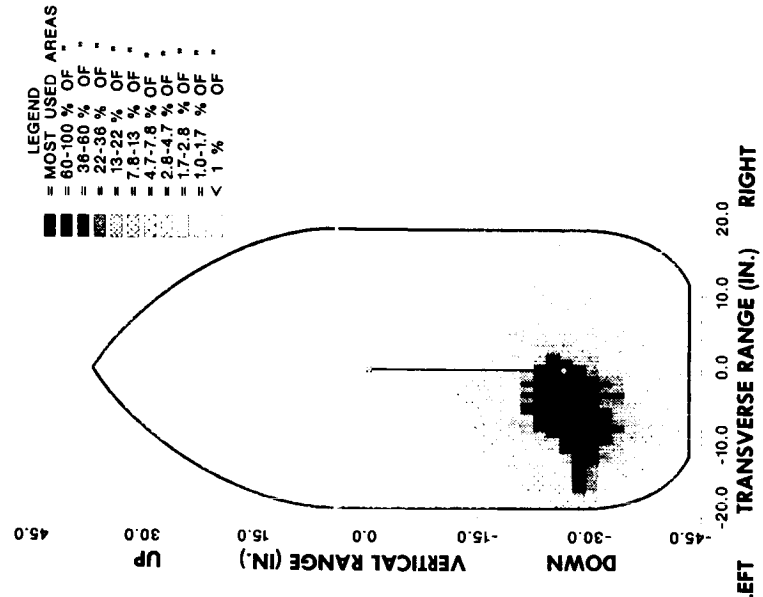

Figure 9. - Wrist position grid--back view.

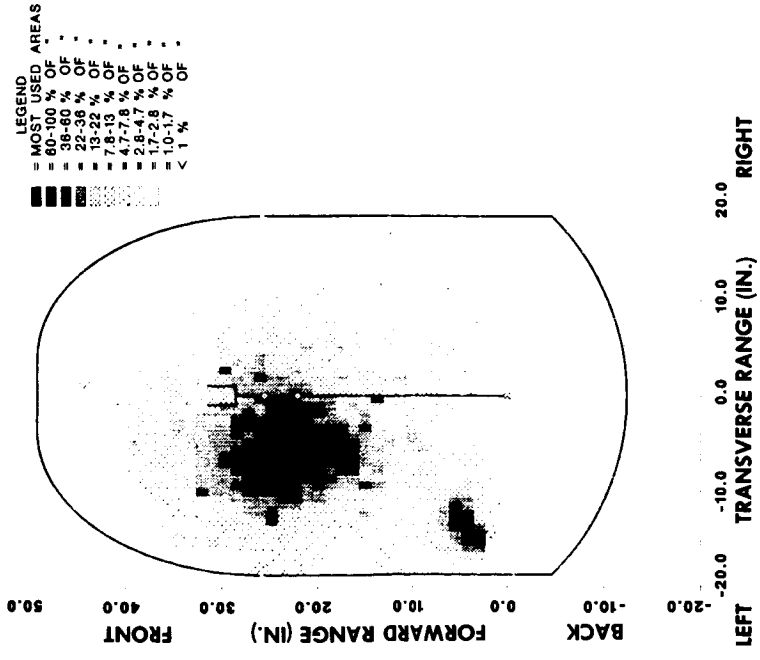

Figure 8. - Wrist position grid--top view.

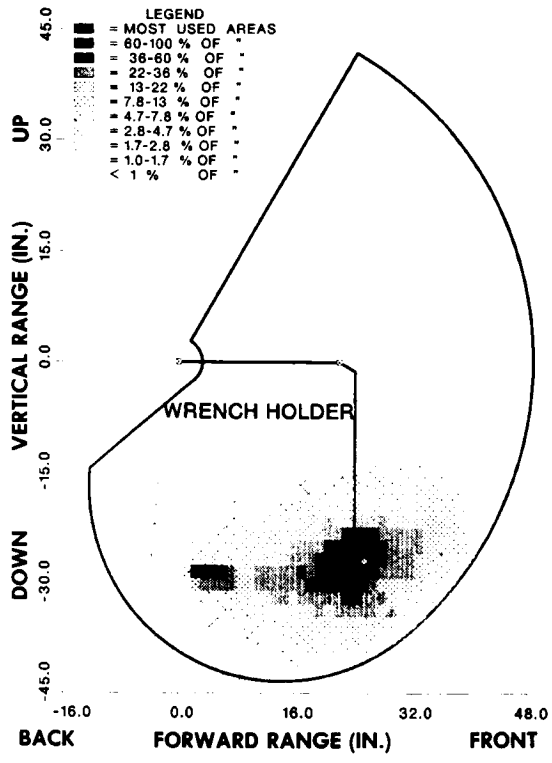

Figure 10. - Wrist position grid--
right side view.

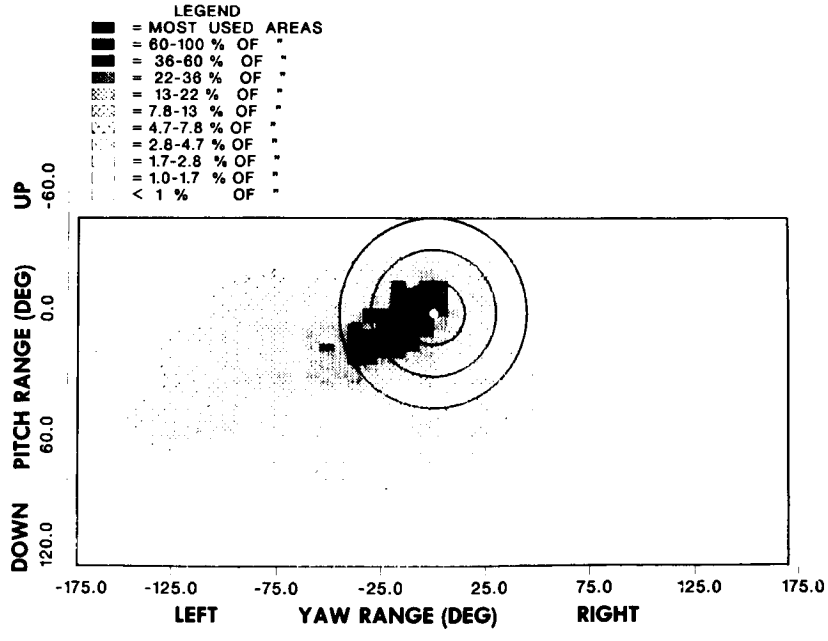

Figure 11. - Wrist orientation grid.

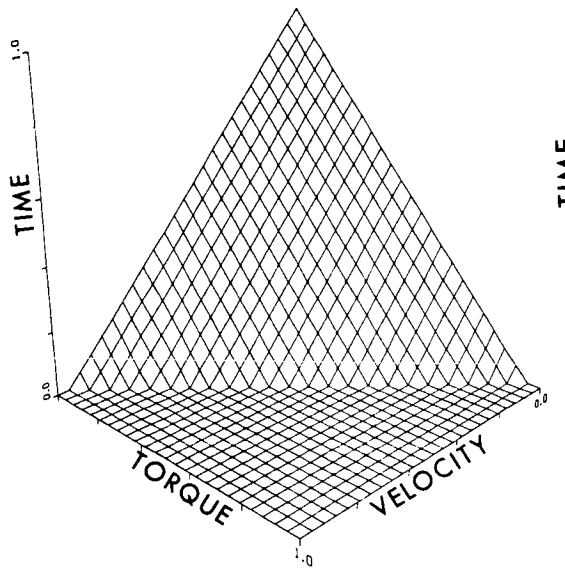

Figure 12. - Ideal mechanical power grid for teleoperators.

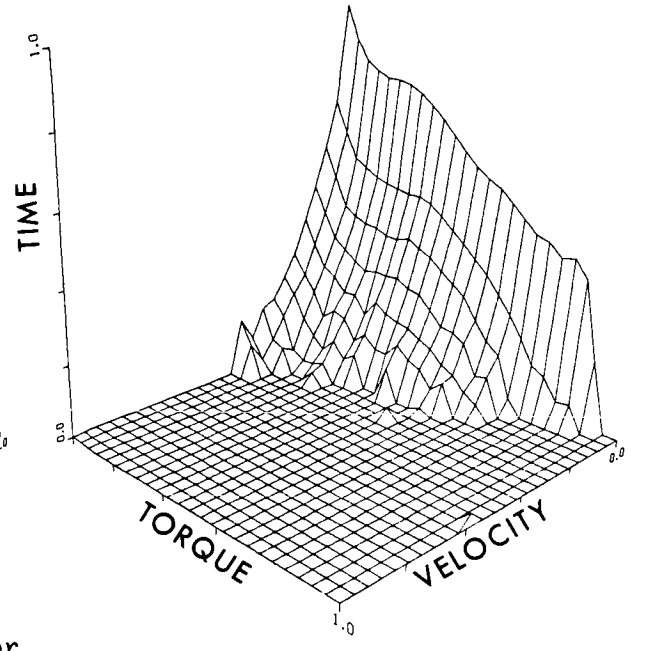

Figure 13. - Mechanical power grid for wrist pitch.

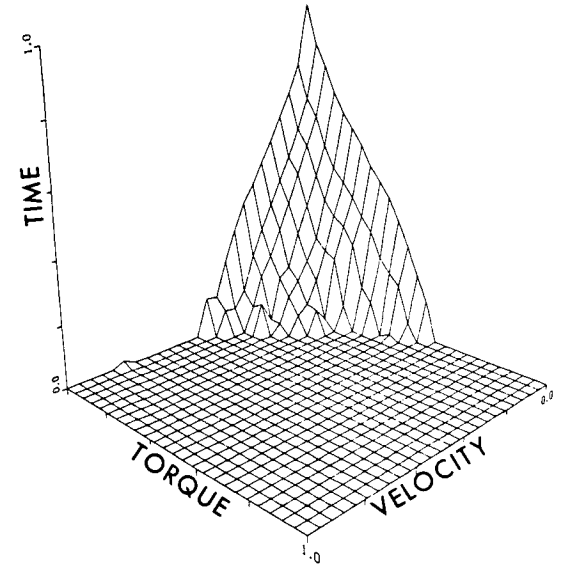

Figure 14. - Mechanical power grid for shoulder roll.

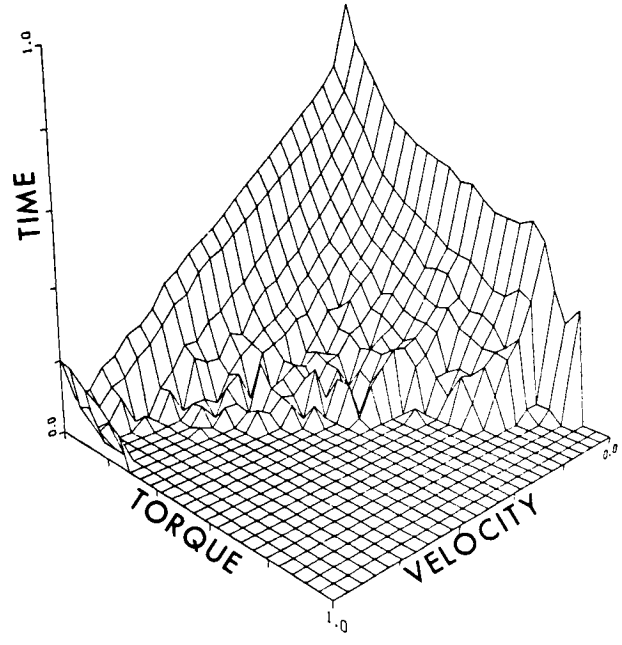

Figure 15. - Mechanical power grid for elbow pitch.

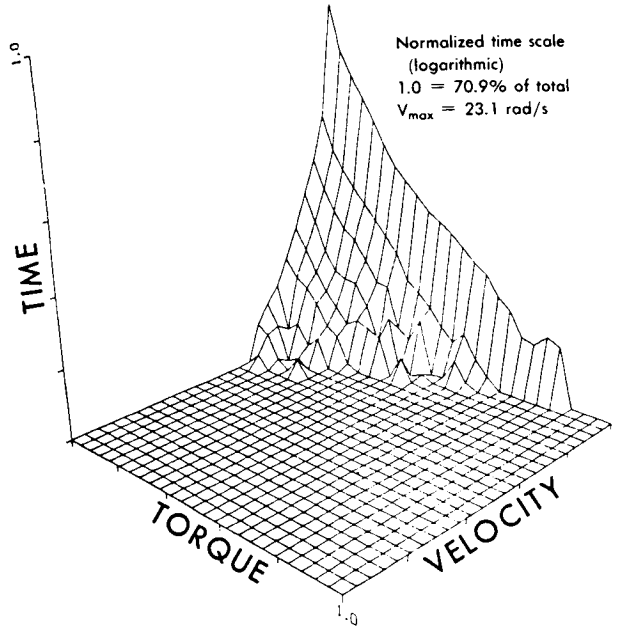

Figure 16. - Mechanical power grid for wrist roll.